Astronomy & Astrophysics manuscript no. swap˙paper˙combined1
March 16, 2011
© ESO 2011

Temperature response of EUV imagers on SOHO, STEREO, SDO and PROBA-2

Claire L. Raftery[1,2], D. Shaun Bloomfield[1], Peter T. Gallagher[1], Daniel B. Seaton[3], David Berghmans[3], and Anik DeGroof[3]

[1] Astrophysics Research Group, School of Physics, Trinity College Dublin, Dublin 2, Ireland.
[2] Space Science Laboratory, UC Berkeley, 7 Gauss Way, Berkeley, CA 94720, USA.
[3] Royal Observatory of Belgium, Solar Physics, Ringlaan 3, B-1180 Brussels, Belgium.

Received:, Accepted:

ABSTRACT

Aims. The temperature response of the 171 Å, Proba-2/SWAP EUV imager was calculated for different solar conditions and compared to those of SDO/AIA, STEREO/EUVI, SOHO/EIT and TRACE.
Methods. Theoretical differential emission measure (DEM) curves were used to generate synthetic spectra within the range 2×10^4 - 5×10^7 K. The convolution of these spectra with the SWAP instrument's wavelength response produced the transmitted spectrum. When integrated over the relevant wavelength range, this resulted in the expected counts per second per pixel at a single temperature i.e. the instrument's sensitivity at a given temperature. This was repeated using CHIANTI-sourced DEM curves for coronal holes, quiet sun, active regions and flares. The procedure was then applied to the five other EUV imagers.
Results. The temperature response to the four solar features varied significantly. The flare response was found to be more than two orders of magnitude greater than the coronal hole response at 1 MK. In addition, the instrument sensitivity to high temperature (>3 MK) plasma was found to be more than six orders of magnitude larger for a flare than a coronal hole, completely distorting the response function. An inter-instrument comparison of the temperature responses revealed them to be in very good agreement, despite significant deviations in their wavelength responses. The similarity of the six instrument responses for each of the four features highlights the stability of the 171 Å passband: although the solar spectrum changes dramatically with temperature, the corresponding temperature response functions remain close to isothermal within the ∼10 Å wide band of sensitivity.

Key words. Space vehicles: instruments – Techniques: image processing – Sun: UV radiation – Sun: atmosphere

1. Introduction

The extreme ultraviolet (EUV) portion of the electromagnetic spectrum is of considerable interest to solar physics because it is dominated by emission lines formed across a wide range of temperatures (Mariska 1993). The steep temperature gradient, from cool ($\sim 10^4$ K), optically thick emission in the chromosphere through to the very hot ($\sim 10^7$ K), highly ionized emission in the corona, means that the entire upper atmosphere emits strongly in the EUV portion of the spectrum. As one of many techniques used for probing the EUV spectrum, imaging telescopes have played a pivotal role in the understanding of the Sun's atmosphere for more than two decades (Underwood et al. 1987).

Imaging telescopes utilize alternating, thin (∼10 Å) layers of molybdinum and silicon on their mirrors to preferentially transmit emission within a certain passband (Windt et al. 2004). A typical passband is sensitive to a spectral range 5-10 Å wide that is integrated across wavelength to give a single intensity value per pixel. Within this range, one or more spectral lines are normally prominent, although their relative contribution to the spectrum may change dramatically with temperature and/or density. Thus, as we image different heights in the corona, the changing density and temperature will result in sometimes dramatically different spectra which in turn result in varying image intensity. This can be accounted for by using differential emission measure (DEM) functions to quantify the amount of emitting material at different temperatures (and therefore heights).

It is not only imaging at various heights that alter the solar spectrum, but also the feature that is being imaged. For example, it is not surprising that the spectrum produced by a coronal hole, known to be cool with low density, is dramatically different to that of a hot, dense solar flare. Therefore, to accurately reproduce the expected transmission from a given passband, consideration must be given to the expected characteristics of the feature of interest (e.g. coronal hole, quiet sun, active region or flare) along with the changing contribution to the spectrum with height in the atmosphere.

In the past, analysis of the temperature response of EUV imagers have been carried out, generally by the instruments' teams (e.g. Delaboudinière et al. 1995; Handy et al. 1999; Howard et al. 2008; Boerner et al. 2011). Typically these investigations have been carried out using a single value (10^{44} cm^{-3}) of emission measure ($EM \propto n_e^2$ where n_e^2 is electron density), thus ignoring the need to account for varying density throughout the corona. More detailed analyses of instrument response function have been carried out by e.g. Del Zanna & Mason (2003) by highlighting the importance of including Fe VIII in the calculation of the Transition Region and Coronal Explorer

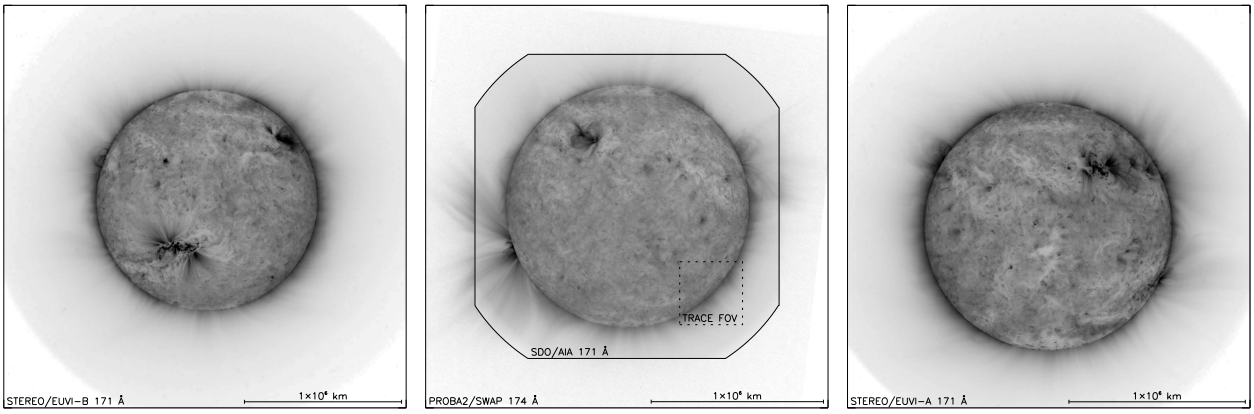

Fig. 1. Comparing the SWAP field of view (centre, large frame) to those of AIA (centre, polygon), TRACE (centre, dotted square), EUVI-A (right) and EUVI-B (left).

(TRACE; Handy et al. 1999) 171 and 195 Å passbands. However, as in the instrument papers, the update was carried out for quiet sun emission at a constant pressure only. Phillips et al. (2005) continued the development of the TRACE temperature response by incorporating the high temperature contribution of the free-free continuum, as predicted by Feldman et al. (1999). Although this analysis was expanded to include emission from quiet sun, active region and flaring plasma, the response curves published by Phillips et al. (2005) were normalised, making them difficult to compare to the responses of other instruments. Brooks & Warren (2006) further improved the temperature response of the TRACE and the Extreme ultraviolet Imaging Telescope (EIT) EUV filters using spectroscopic observations taken with the Coronal Diagnostic Spectrometer (CDS). Recalculating the ionisation fractions using the CDS data facilitated a more accurate calculation of the instruments' temperature response curves compared to those in the instrument papers. As before, the analysis was conducted only for quiet sun emission. It is clear that while there have been significant improvements made, studies carried out in the past do not facilitate the *direct* comparison of multiple instruments or different types of plasma.

In this paper, version 6 of the CHIANTI atomic physics package (Dere et al. 1997, 2009) is used to investigate the temperature response of six solar instruments in the commonly termed "171 Å" wavelength band. These responses are calculated for four classes of solar plasmas: coronal holes (CH), quiet sun (QS), active regions (AR) and solar flares (FL). The variation of EM with height is taken into account through the use of DEM functions. The instruments under investigation and their corresponding wavelength responses are described in §2.1. The calculation of isothermal spectra and the nature of the transmitted spectra are presented in §2.2. The resulting temperature response curves for the four solar conditions and for the six instruments are described in detail in §3. Finally, the conclusion and implications of this study are discussed in §4.

2. Method

2.1. Instruments and wavelength responses

There are six instruments under investigation in this paper: the EIT on board the Solar and Heliospheric Observatory (SOHO; Delaboudinière et al. 1995), the TRACE telescope, the twin Extreme ultraviolet Imagers on board the Solar Terrestrial Relations Observatory (STEREO/EUVI; Howard et al. 2008), the Atmospheric Imaging Assembly on board the Solar Dynamics Observatory (SDO/AIA; Boerner et al. 2011) and finally, the recently launched Sun Watcher using Active Pixel System detector and image processing instrument on ESA's Proba-2 satellite (Proba2/SWAP; Berghmans et al. 2006).

SWAP is an imaging telescope consisting of a single 171 Å filter with a field of view (FOV) of $54' \times 54'$ (see Figure 1 and Table 3.1 for comparison to other instruments). With its remarkable ability to off-point to exclude the solar disk, this unique instrument provides images of the EUV corona out to 2 $R_\odot$. The high cadence of the instrument (1 image per minute) will facilitate the investigation of fast moving phenomena such as CMEs and EIT "waves". This will be especially important in the coming years as the STEREO spacecraft progress further in their orbits. SWAP, with its similar capabilities, will be an excellent extension to the EUVI instruments.

Launched in 2006, the EUVI instruments on STEREO A and B are full-disk imagers with a FOV comparable to SWAP. These twin spacecraft have image cadence of >2 minutes and high spatial resolution with a plate scale of $1.6''$/pixel. The instruments have four EUV filters each (171, 195, 284 and 304 Å) and have provided users with the first EUV stereo images of the Sun. Although the two STEREO spacecraft provide a unique and important dual-view of the sun, as they progress in their orbits away from the Earth, these instruments will no longer be useful for on-disk (as seen from Earth) observations.

EIT has often been used as a "third eye" in multi-view analysis concerning the EUVI instruments. With significant heritage and the same filters as EUVI, it can provide a complementary or comparative view of an event (e.g. Krista & Gallagher 2009; Raftery et al. 2010). EIT has significantly reduced cadence and spatial resolution compared to the newer instruments. However, as a pioneer in the field of solar EUV imaging, it was once revolutionary in its capabilities.

TRACE has also transformed solar physics using its seven passbands, 3 of which are in the EUV range (171, 195 and 284 Å). Unlike other EUV telescopes, the TRACE FOV is not full-disk. Rather, it achieves extremely high res-

Instrument	Plate scale [arcsec/pixel]	Nominal cadence [Minutes]	FOV [arcmin]	Aperture area [cm^2]
SWAP	3.1	1	54^2	8.55
EUVI	1.6	>2	43^2	301
EIT	2.6	10	45^2	12
TRACE	0.5	<1	8.5^2	706
AIA	0.6	<1	41^2	314

Table 1. Specifications for the EUV instruments used in this investigation.

olution (0.5″pixels) in a FOV of 8.5′×8.5′. Combined with a cadence of less than one minute, this instrument has revealed small scale solar features that had never been seen before. TRACE also deviated from other imagers in the type of detector used. Unlike the other instruments listed here, TRACE utilised a front-illuminated CCD which reduced its overall sensitivity. This does not however, affect the very high quality of the images TRACE produces.

The AIA instrument has significant heritage from TRACE, although it has reverted to the use of a full-disk, back-illuminated structure. This instrument has yet again revolutionized solar physics. With resolution comparable to TRACE thanks to a very large aperture area, nine EUV passbands (94, 131, 171, 193, 211, 304, 335 Å), full-disk resolution and a cadence of less than a minute, AIA has revealed the solar corona in more detail than ever before.

The wavelength responses, $R(\lambda)$, of the instruments listed above are shown in Figure 2. The first deviation of note is the offset in the wavelength responses' magnitude. As expected, the TRACE response is the lowest of all, mainly due to the low efficiency of its detector and its small FOV. Despite its similarity to TRACE, AIA has the highest response. The shape of the AIA response is also significantly different to the others. This is a testament to both its large aperture size and the developments in technology since TRACE was built. The EUVI and EIT instruments have very similar responses despite their significantly different aperture sizes. This again, may be attributed to developments in the efficiency of modern detectors. SWAP falls between TRACE and EUVI/EIT due to a combination of its small aperture size and the nature of an APS detector reducing its overall sensitivity.

Moving through increasing wavelength, it is interesting to note that all instruments have a gradual increase in their $R(\lambda)$ over the first 5±1 Å of the wavelength response function. It is not surprising that SWAP and EUVI (and EIT, to a certain extent) have a similar slope in this regime since these instruments share similar development techniques. From ∼170 Å the instruments' responses begin to deviate. SWAP, EUVI B, EUVI A and EIT have a very sharp rise between 170 and 171 Å, peaking at (1.2, 7.0, 8.5, 11.3)×10^{-12} DN phot^{-1} cm^2 str pix^{-1} respectively. Each of these four responses "plateau" and remain at near constant values for 6±2 Å. The TRACE and AIA responses however, have a significantly different shape. While the AIA response has a similarly sharp rise to its peak value of 2.7×10^{-11}, the maximum sensitivity occurs at 172 Åand has much sharper peak (∼2 Å wide). The TRACE response also has a narrow peak, at ∼4 Å wide, although the rise to the maximum sensitivity of 2.5×10^{-13} is far more gradual than the other instruments. The TRACE and EIT responses decrease smoothly to ∼188 Å at which point they level off. The SWAP, EUVI A and EUVI B all have a steeper decay rate between ∼180 - 184 Å and experience a secondary peak between ∼184 and 192 Å.

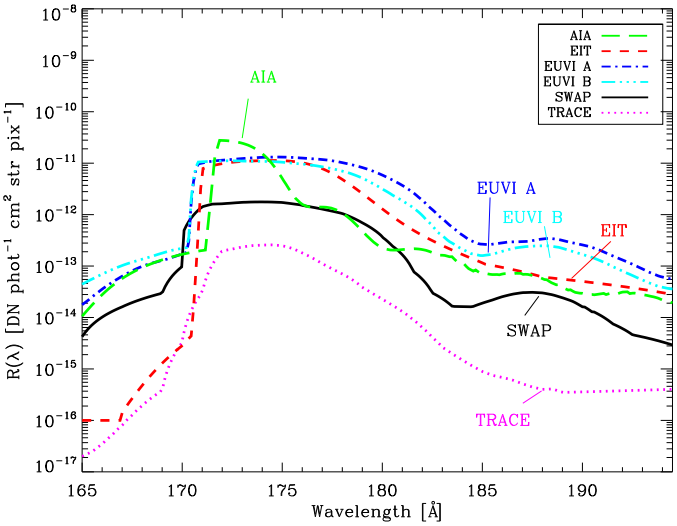

Fig. 2. Wavelength response of AIA (green), EIT (red), EUVI A (blue), EUVI B (pale blue), SWAP (black) and TRACE (purple).

2.2. Synthetic spectrum calculation

The method presented here calculates the temperature response of an EUV imager between the temperatures of 2×10^4 and 5×10^7 K using four different DEM curves (Figure 3). The column emission measure (EM) is defined as the amount of emitting plasma in a column dh. This is one property required by the CHIANTI routines for this analysis and can be written as:

$$EM = \int n_e^2 dh, \tag{1}$$

Since $DEM = n_e^2(dh/dT)$, we can redefine the EM to be:

$$EM = \int_{\Delta T} DEM dT \tag{2}$$

The EM can therefore be extracted from the DEM curve for a temperature bin of $\log_{10}\Delta T = 0.1$. The curves used in this study, obtained from CHIANTI, are shown in Figure 3. The CH, QS and AR curves for both EM and DEM are very similar up to a temperature of ∼6×10^5 K. This roughly corresponds to the temperature at which the CH EM curve peaks. Following the split, the CH curves rapidly decrease, marking the little or no plasma present in a CH at temperatures above 1 MK. The QS and AR curves peak

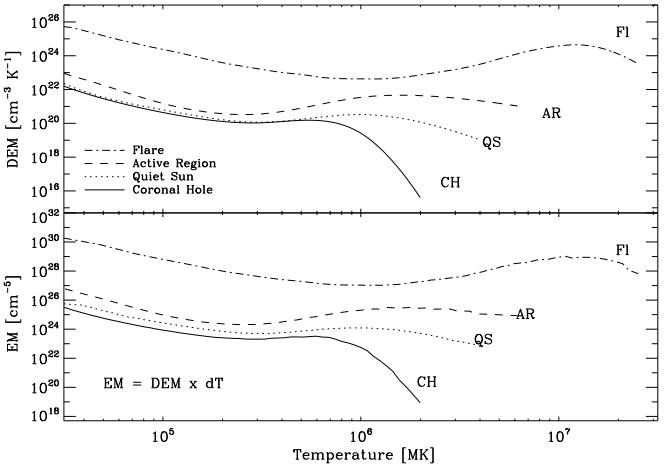

Fig. 3. Differential emission measure and emission measure as a function of temperature for coronal hole, quiet sun, active region and flare.

soon after at a temperature of ∼1.6 MK and ∼2 MK respectively, although the AR curves have a significantly slower decay, remaining close to constant until close to 5 MK. The FL curves show a marked difference in comparison to the other three. The trough that occurs close to 1.5×10^5 K in the other three classes of emission is observed at ∼1 MK in the FL case. In addition, the DEM and EM peaks occur at a much higher temperature of ∼10 MK. It is interesting to note that the FL trough occurs at approximately the same temperature as the AR peak. This suggests that during a solar flare, the plasma within an active region loop is heated to very high temperatures (∼10^7 K), thus leaving the active region loops devoid of 1 MK plasma.

Along with T and EM values, the abundances were taken to be those of Feldman et al. (1992) and the ionization fractions of Mazzotta et al. (1998) were used. A generic density value was also supplied. The intensity of an emission line depends on the population of the upper levels of the atomic transition, which itself depends on the plasma density. Although this parameter has little effect on the overall spectrum, the following density values were used, one for each emission class:

- Coronal hole: 10^7 cm^{-3} (Wilhelm 2006)
- Quiet sun: 6×10^8 cm^{-3} (Young 2005)
- Active region: 5×10^9 cm^{-3} (Gallagher et al. 2001)
- Flare: 10^{11} cm^{-3} (Raftery et al. 2009)

Figure 4 provides a schematic diagram of the process applied to generating the temperature response curves. At a given temperature, T_i, the corresponding EM_i is obtained (Figure 4a, asterisk) and used to calculate an "isothermal" spectrum using CHIANTI (Figure 4b). Each isothermal spectrum is then multiplied by the wavelength response of an instrument (SWAP in the case of Figure 4c) to give the expected throughput of the instrument: the transmitted spectrum (Figure 4d). The transmitted spectrum is the number of counts (or DN) a single pixel is expected to detect in one second at a given wavelength. Integrating the transmitted spectrum across the wavelength range 165 - 200 Å for a particular T_i results in the instrument's response at a that temperature (Figure 4e, asterisk). Repeating this process for all temperatures results in a smooth temperature response function (Figure 4e).

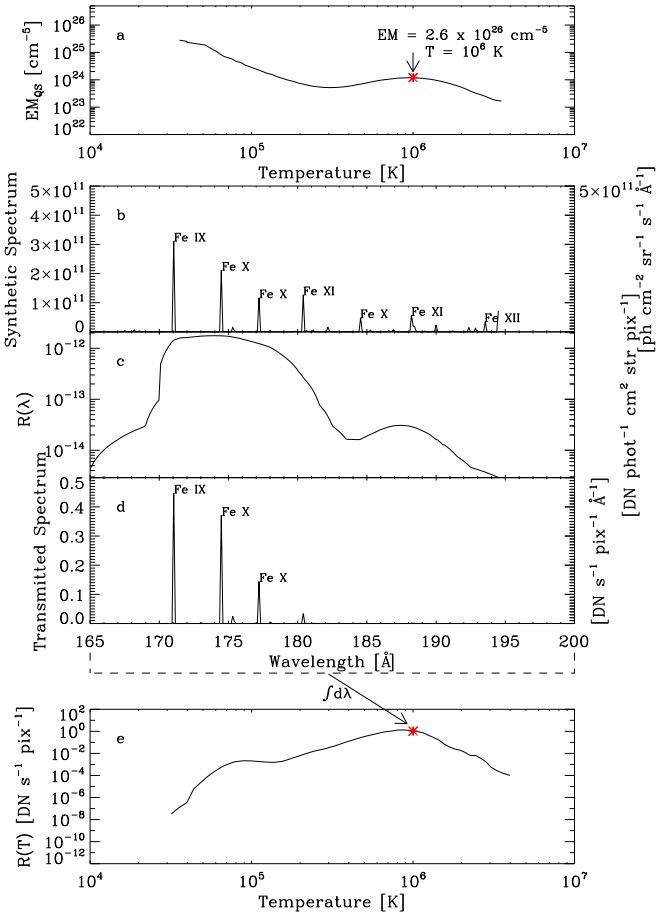

Fig. 4. (a) Quiet sun EM curve with a single point highlighted at T = 10^6 K and EM = 2.6×10^{26} cm^{-5}. (b) Synthetic isothermal spectrum calculated for the conditions selected in panel (a). (c) The SWAP $R(\lambda)$ function. (d) Transmitted spectrum from the product of (b) and (c). (e) The SWAP temperature response, calculated by integrating the transmitted spectrum over wavelength. The asterisk corresponds to the conditions set in panel (a).

The method used for calculating the response spectrum has been verified by comparing the total emission from spectra across all temperatures to the total emission from a single spectrum calculated using the corresponding DEM function. The results are correct to within ±0.2%.

Figure 5 shows stacked transmitted spectra for SWAP, EUVI A and AIA i.e. colour corresponds to the transmitted spectrum line intensity across wavelength (x axis) at all temperatures within the range of interest (y axis). From top to bottom, these psuedo-spectragrams are calculated for flares (scaled down by a factor of 100), active regions, quiet sun and coronal hole (scaled up by a factor of 10) conditions. There are many features to note, including the 171 Å Fe IX line, present in all cases for SWAP and EUVI between 0.3 and 1.25 MK (pink/white line at 171 Å). It is important to recognize the diminished intensity of this line in the AIA response. This is due to the shifted wavelength response of this instrument (see §2.1). The Fe X lines at 174.5, 175.3 and 177.2 Å formed around 1 MK are visible with the 174.5 and 177.2 Å lines around 20% brighter than

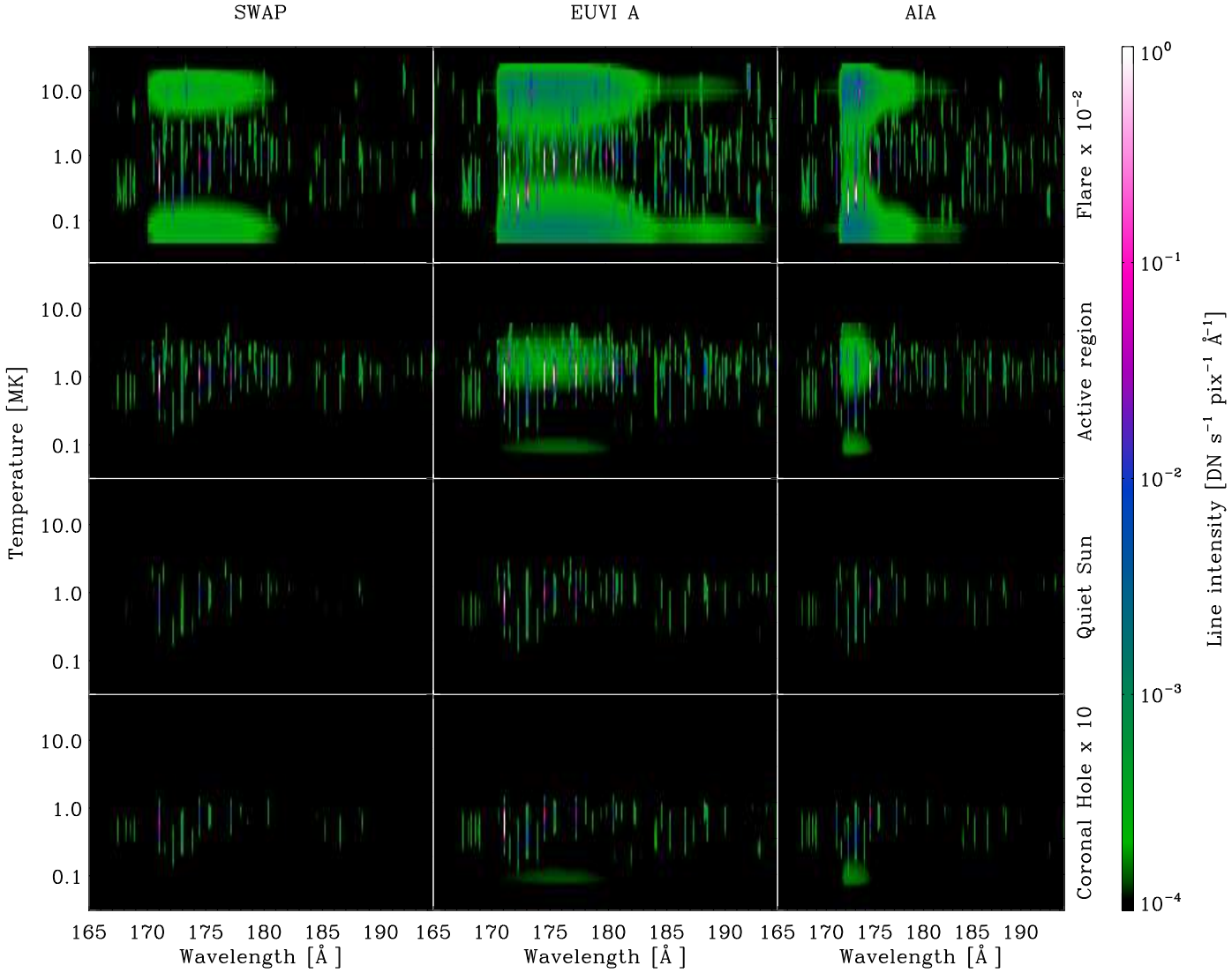

Fig. 5. Response of SWAP (left), EUVI A (middle) and AIA (right) to temperature before wavelength integration i.e. the expected transmitted spectrum for each temperature. Color corresponds to intensity of the temperature response.

the 175 Å line. It can be seen that many of the hot lines that appear bright in the AR and FL cases are diminished in intensity for AIA. This is due to the sharply peaked nature of the instrument response.

The continuum at both low and high temperatures can be observed clearly in this figure, in particular for the flare cases. The low temperature continuum is present around 10^5 K in all cases, although in the CH, QS and to come extent, the AR case, it is of low intensity. Despite this, it has a significant integrated contribution to the spectrum between 170 and 180 Å. The high temperature continuum however, is observed only in AR and FL conditions and has comparable brightness to the 192 Å Fe XXIV line (50%). In the flaring case, it is clear that the levels of high and low temperature continuum are also at similar levels. It should be noted however, that the low temperature continuum level in the flare case is 500 times greater than in the coronal hole case. Although this may be due to the some four orders of magnitude difference in the EM curves for these conditions, this still highlights the significant contribution the continuum makes to the spectrum during solar flares.

3. Results

Figures 5 and 6 shows the temperature response of the instruments under consideration in this paper, although only the responses of SWAP, EUVI A and AIA are displayed in Figure 5. Table 3.1 shows the expected pixel values for each telescope for each of the four conditions.

3.1. Solar feature comparison

In Figure 6, the temperature response of all instruments for coronal hole (a), quiet sun (b), active region (c) and solar flare (d) can be seen. It is apparent that the responses of the instruments to these different features are significantly

Instrument	Coronal Hole $[DNs^{-1}pix^{-1}]$	Quiet Sun $[DNs^{-1}pix^{-1}]$	Active Region $[DNs^{-1}pix^{-1}]$	Flare $[DNs^{-1}pix^{-1}]$
SWAP	2.2	12.9	1.5×10^2	1.5×10^4
EUVI A	10.5	65.0	7.9×10^2	7.7×10^4
EUVI B	10.1	57.8	6.7×10^2	6.7×10^4
EIT	12.4	73.5	8.7×10^2	8.6×10^4
TRACE	0.1	0.8	0.1×10^2	0.1×10^4
AIA	3.2	23.7	3.1×10^2	4.9×10^4

Table 2. Expected counts per pixel for each of the instruments for each solar condition.

different, as expected. The CH response has a primary peak at 7.5×10^5 K, a temperature only slightly higher than the EM peak in Figure 3. This is not surprising since the coronal hole EM never rises above 1 MK (the formation temperature of the characteristic Fe IX/X lines). Rather, in the CH case, the combined contribution from the oxygen lines formed at $\lambda < 170$ Å and low temperature continuum is greater than that of the Fe IX/X lines. This is not the case for the other conditions: the intensity of the Fe IX/X lines is significantly greater in all other cases.

As expected, the QS response is more sensitive than the CH response due to the larger quantity of emission observed in these cases (cf Figure 3). More interestingly, the levels of sensitivity at higher temperature increases with the formation of a "shoulder" at ∼3 MK. This is further emphasized in the AR response, due to rising levels of hot continuum and the abundance of hot lines. The overall increase in the AR response magnitude is more than an order of magnitude greater than the QS response. Finally, the FL temperature response is the most dramatic of all. Unlike the highly peaked response functions observed in all other cases, each response is within an order of magnitude of the peak value. For example, the sensitivity of SWAP at 10^5, 10^6 and 10^7 K are 53.8, 697.2, 77.7 respectively. Comparing this one order of magnitude difference to that of quiet sun (two orders of magnitude) and active region (three orders of magnitude), we can see the significance of the high continuum levels.

3.2. Inter-instrument comparison

The temperature responses for each of the four solar conditions are shown in Figure 6 for all six instruments. In order to compare the response functions of each instrument, we shall focus on panel d of this figure. Considering the significant deviations noted in the respective wavelength responses in §2.1 (Figure 2), the correlation between the various temperature responses are remarkable. However, there are some discrepancies worth noting.

- Between (2-4)$\times10^5$ K, there is an increase in the relative sensitivity of AIA and TRACE compared to SWAP, EIT and EUVI. Since the peak of both AIA and TRACE's wavelength responses occur at ∼172 Å, they are more sensitive to the O V lines that are formed around 172 Å between 0.2 and 0.5 MK, thus biasing their $R(T)$ value to lower temperatures.
- At temperatures between ∼0.2-0.6 MK, there is a significant trough in the TRACE and AIA temperature response functions. This is due to the sharply peaked nature of their wavelength response. Comparing the EUVI A and AIA columns in Figure 5 flare plots, it is clear that there is a significant difference in continuum lev-

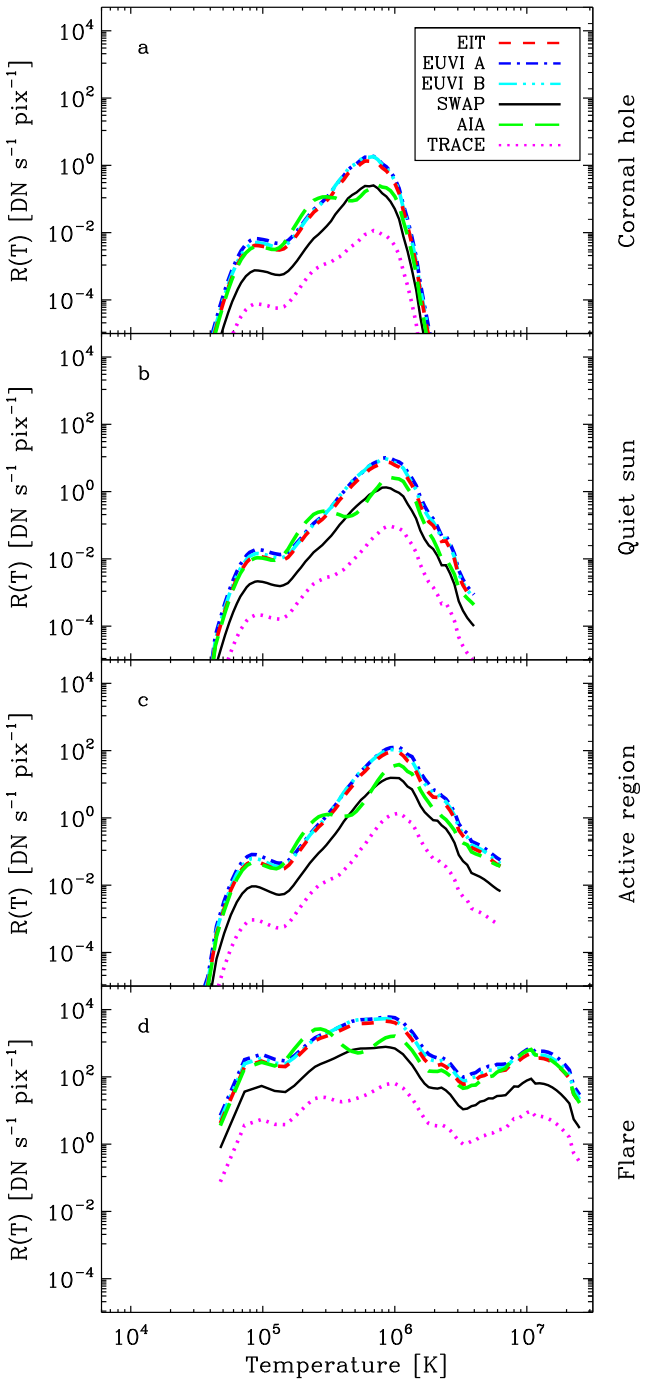

Fig. 6. Instrument response to temperature for six EUV imagers in the 171 Å passband for (a) coronal hole, (b) quiet sun, (c) active region and (d) flare.

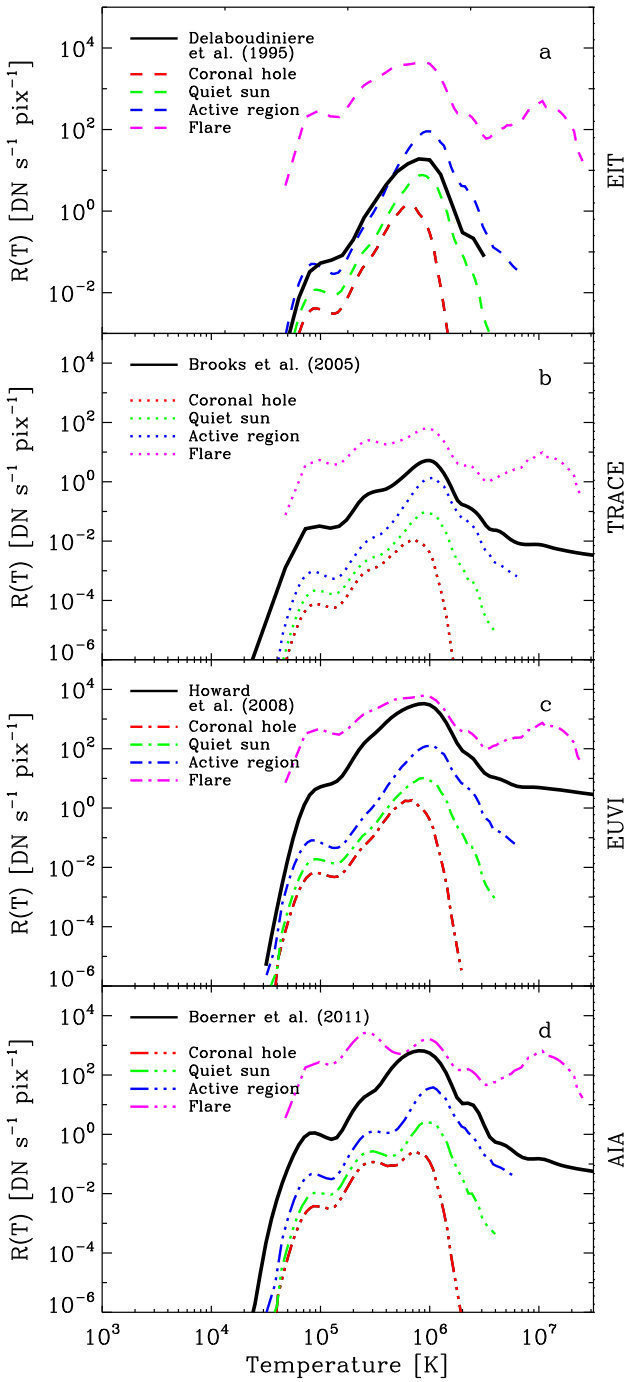

Fig. 7. Comparison of our results to those of the instrument teams (available on SSWIDL) for EIT (a), TRACE (b), EUVI (c) and AIA (d). The instrument teams results are shown in black while our coronal hole, quiet sun, active region and flare results are shown in red, green, blue and purple respectively.

els between 175 and 180 Å at these temperatures, with AIA showing much lower sensitivity to low temperature continuum in this region of the passband.

– Finally, it can be seen that SWAP and both EUVI instruments have a subtle increase between 4-6×10^6 K. These telescopes are more sensitive to emission lines formed between 183 and 190 Å due to the secondary bump in their wavelength response. This is primarily due to the increased continuum levels the secondary bump accommodates. These faint features can be seen in the first and second column of Figure 5.

3.3. Comparison to instrument papers

As discussed in §1, the temperature response functions for these instruments have previously been examined by the instrument teams. A comparison to these response functions was carried out and is presented in Figure 7. Note, the SWAP response is not discussed in Figure 7 as the results presented here are used in the SWAP instrument paper. Each panel contains the $R(T)$ from the instrument team (black line) and the $R(T)$ curves calculated in this paper for the four solar classes of emission.

Beginning with the EIT plots in panel (a), it is clear that below ∼10^5 K, the $R(T)$ calculated by Delaboudinière et al. (1995) is in good agreement with our AR response curve. It is worth nothing the small difference in response shape at 10^5 MK.This is most likely to do with the fact that when this analysis was conducted, the low temperature continuum levels were not as well understood (Feldman et al. 1999). As the temperature increases, the Delaboudinière response falls between the quiet sun and active region responses. A small high temperature bump is noted at $\sim$ 2.5 MK, although only 10% of the corresponding AR value. At no stage does the response take into account the high temperature contribution observed during flares. The Delaboudinère response to temperatures above 2×10^6 K is not available.

The $R(T)$ calculated by Brooks & Warren (2006) for the TRACE instrument is shown in panel b. The temperature response available through SSW has been calculated in the units of $DNs^{-1}cm^3$. Since the calculation was made using an emission measure value of 10^{44} cm^3, we have scaled the response function correspondingly. It is clear that the response curve accounts for emission around 1 MK during active phenomena more accurately than EIT. In addition, the response at lower temperatures falls between our active region and flare responses and is in reasonable agreement with the overall shape of our AR curves up to 1 MK. Finally, while the high temperature response ($>$ 2 MK) lies within between our AR and FL results, the structure observed in our flare curve is not seen in the Brooks curve. This is most likely due to the constant emission measure value used to calculate the Brooks response. This does not account for the larger amount of hot coronal plasma that may be observed during flares. Instead, by assuming the volume will remain constant, the response at high temperatures is flat.

The responses of the EUVI instrument are shown in panel (c) with comparison to those in Howard et al. (2008). The Howard response shows similar trends to that of TRACE: falling between our AR and FL responses with a peak comparable to our flare peak at 1 MK. Again and for the same reasons as the Brooks/TRACE response, the high temperature response from Howard remains flat.

Finally, the AIA responses are shown in panel (d) and compared to results from Boerner et al. (2011). Similar to TRACE, it was necessary to scale the Boerner response function by the emission measure. As before, the instrument team's response falls between our flare and active region curves. At low temperatures, despite the offset, the shape of the Boerner response curve is in good agreement with our results with many of the smaller bumps visible in all curves. This is a testament to developments in atomic

physics, specifically within the CHIANTI packages. As in the previous cases, the high temperature response is almost level above 2 MK.

It is clear from these plots that while the response curves supplied for these instruments make a good approximation to the response of the average sun, in more extreme cases, they completely break down. Although for the most part, a reasonable attempt to account for flaring emission at ∼1 MK is made, the response of the instruments to coronal holes or even to quiet sun is largely overestimated.

4. Conclusions

This paper studies the temperature response of the SWAP EUV imager, along with five similar instruments in the 171 Å passband. The temperature responses were calculated for four different solar features: coronal holes, quiet sun, active regions and flares. Besides an expected offset in the magnitudes of the temperature responses, the six instruments were found to agree remarkably well, despite significant deviations in their wavelength response functions. Any differences that occurred in the temperature responses were accounted for by considering the shape of the wavelength responses. This is a testament to the homogenous nature of the spectrum within the 171 Å sensitivity range. The revelation comes from comparing the various instruments response functions for a variety of solar conditions. In an expansion on previous works (e.g. Phillips et al. 2005; Brooks & Warren 2006; Del Zanna & Mason 2003), we analyzed the response for four different solar conditions. It was found that there was significant differences between the "quiet" features (i.e. coronal holes and quiet sun) and "active" features - active regions and flares. The most striking difference is the high temperature response of this passband. Although known for their response to ∼1 MK plamsa, 171 Å passband imagers may also observe emission at higher temperatures, up to 8 MK in extreme cases, provided the volume of emitting plasma is high enough. The spectral contribution from high temperature continuum and highly ionized iron in this wavelength range is non-negligable. Although this will not have too great an effect for medium sized events, it is something that should be given consideration during large M and X class flares.

Additionally, the ability to compare the responses of individual instruments is important to understanding both similarities and differences in co-ordinated observations. Presently there exists comparisons between the TRACE and EIT instruments. This is understandable since these two instruments have been at the forefront of EUV imaging until very recently. However, with the retirement of these instruments and the introduction of four new imagers in almost as many years there is a clear need to expand the instrument comparison. While the individual response functions are available in their respective instrument papers, different units, methods and initial conditions in their calculation make comparison difficult. In addition, the instruments' temperature response functions are, in general, presented for only one solar feature - usually quiet sun. Here we present a solution to this problem by combining an in-depth study of multiple instruments and different solar conditions.

This paper presents a new method of calculating the temperature response of EUV imagers to different types of solar conditions. This method takes account of deviations in the solar spectrum with different features/conditions. It can be used for any DEM and can be applied to multiple instruments, thus facilitating their direct comparison. In addition, the method can be easily adapted to investigate other passbands besides 171 Å, along with new instruments in the future. This work will facilitate a more precise understanding and interpretation of EUV images. It will be expanded by incorporating real DEM functions calculated using the Extreme Ultraviolet Variability Experiment (EVE) on board SDO in an attempt to generate more realistic results for different conditions.

Acknowledgements. This work was supported by an ESA/Prodex grant administered by Enterprise Ireland. DSB is supported by the European Community (FP7) under a Marie Curie Intra-European Fellowship for Career Development. Support for DBS came from PRODEX grant no. C90345 managed by the European Space Agency in collaboration with the Belgian Federal Science Policy Office (BELSPO) in support of the PROBA2/SWAP mission, and from the European Commissions Seventh Framework Programme (FP7/2007-2013) under the grant agreement no. 218816 (SOTERIA project, www.soteria-space.eu). SWAP is a project of the Centre Spatial de Liege and the Royal Observatory of Belgium funded by the Belgian Federal Science Policy Office (BELSPO)

References

Berghmans, D., et al. 2006, Advances in Space Research, 38, 1807
Boerner, P., Edwards, C., Lemen, J., Rausch, A., Schrijver, C., Shine, R., Shing, L., Stern, R., Tarbell, T., Title, A. & Wolfson, C. J. 2011, *in prep*
Brooks, D. H., & Warren, H. P. 2006, ApJS, 164, 202
Delaboudinière, J.-P., et al. 1995, Sol. Phys., 162, 291
Del Zanna, G., Bromage, B. J. I., & Mason, H. E. 2003, A&A, 398, 743
Del Zanna, G., & Mason, H. E. 2003, A&A, 406, 1089
Dere, K. P., Landi, E., Mason, H. E., Monsignori Fossi, B. C. &Young, P. R. 1997, A&AS, 125, 149
Dere, K. P., Landi, E., Young, P. R., Del Zanna, G., Landini, M., & Mason, H. E. 2009, A&A, 498, 915
Domingo, V., Fleck, B., & Poland, A. I. 1995, Space Science Reviews, 72, 81
Doschek, G. A., Laming, J. M., Feldman, U., Wilhelm, K., Lemaire, P., Schuehle, U., & Hassler, D. M. 1998, ApJ, 504, 573
Feldman, U., Mandelbaum, P., Seely, J. F., Doschek, G. A., & Gursky, H. 1992, ApJS, 81, 387
Feldman, U., Laming, J. M., Doschek, G. A., Warren, H. P., & Golub, L. 1999, ApJ, 511, L61
Gallagher, P. T., Phillips, K. J. H., Lee, J., Keenan, F. P., & Pinfield, D. J. 2001, Astrophysical Journal, 558, 411
Guhathakurta, M., Fludra, A., Gibson, S. E., Biesecker, D., & Fisher, R. 1999, Journal of Geophysics Research, 104, 9801
Handy, B. N., et al. 1999, Sol. Phys., 187, 229
Harrison, R. A., Sawyer, E. C., Carter, M. K. et al. 1995, Sol. Phys., 162, 233
Hochedez, J.-F., et al. 2006, Advances in Space Research, 37, 303
Howard, R. A., et al. 2008, Space Science Reviews, 136, 67
Kaiser, M. L., Kucera, T. A., Davila, J. M., St. Cyr, O. C., Guhathakurta, M., & Christian, E. 2008, Space Science Reviews, 136, 5
Krista, L. D., & Gallagher, P. T. 2009, Sol. Phys., 256, 87
Landi, E., & Phillips, K. J. H. 2006, ApJS, 166, 421
Lawrence, G., et al. 2005, Solar Wind 11/SOHO 16, Connecting Sun and Heliosphere, 592, 685
Mariska, J. T. 1993, The Solar Transition Region, by John T. Mariska, pp. 290. ISBN 0521382610. Cambridge, UK: Cambridge University Press, January 1993.,
Mazzotta, P., Mazzitelli, G., Colafrancesco, S., & Vittorio, N. 1998, A&AS, 133, 403
Pesnell, W. 2008, 37th COSPAR Scientific Assembly, 37, 2412
Phillips, K. J. H., Chifor, C., & Landi, E. 2005, ApJ, 626, 1110
Raftery, C. L., Gallagher, P. T., Milligan, R. O., & Klimchuk, J. A. 2009, A&A, 494, 1127
Raftery, C. L., Gallagher, P. T., McAteer, R. T. J., Lin, C.-H. & Delahunt, G.,. 2010, ApJ, *in review*

Schrijver, C. J., et al. 1999, Sol. Phys., 187, 261
Seaton, D., et al. 2009, *in prep*
Underwood, J. H., Bruner, M. E., Haisch, B. M., Brown, W. A., & Acton, L. W. 1987, Science, 238, 61
Vernazza, J. E., Avrett, E. H., & Loeser, R. 1981, ApJS, 45, 635
Warren, H. P., Bookbinder, J. A., Forbes, T. G., Golub, L., Hudson, H. S., Reeves, K., & Warshall, A. 1999, ApJ, 527, L121
Wilhelm, K. 2006, A&A, 455, 697
Windt, D. L., Donguy, S., Seely, J. F., Kjornrattanawanich, B., Gullikson, E. M., Walton, C. C., Golub, L., & DeLuca, E. 2004, Proc. SPIE, 5168, 1
Young, P. R. 2005, Astronomy and Astrophysics, 444, L45